# Role of Bioactive 3D Hybrid Fibrous Scaffolds on Mechanical Behavior and Spatiotemporal Osteoblast Gene Expression

Bedilu A. Allo,[†] Shigang Lin,[†] Kibret Mequanint,[†,‡,*] and Amin S. Rizkalla[†,‡,§,*]

[†]Department of Chemical and Biochemical Engineering, [‡]Biomedical Engineering Graduate Program, and [§]Schulich School of Medicine and Dentistry, The University of Western Ontario, London, Ontario, Canada N6A 5B9

ABSTRACT: Three-dimensional (3D) bioactive organic—inorganic (O/I) hybrid fibrous scaffolds are attractive extracellular matrix (ECM) surrogates for bone tissue engineering. With the aim of regulating osteoblast gene expression in 3D, a new class of hybrid fibrous scaffolds with two distinct fiber diameters (260 and 600 nm) and excellent physico-mechanical properties were fabricated from tertiary (SiO_2—CaO-P_2O_5) bioactive glass (BG) and poly (ε-caprolactone) (PCL) by in situ sol—gel and electrospinning process. The PCL/BG hybrid fibrous scaffolds exhibited accelerated wetting properties, enhanced pore sizes and porosity, and superior mechanical properties that were dependent on fiber diameter. Contrary to control PCL fibrous scaffolds that were devoid of bonelike apatite particles, incubating PCL/BG hybrid fibrous scaffolds in simulated body fluid (SBF) revealed bonelike apatite deposition. Osteoblast cells cultured on PCL/BG hybrid fibrous scaffolds spread with multiple attachments and actively proliferated suggesting that the low temperature in situ sol—gel and electrospinning process did not have a detrimental effect. Targeted bone-associated gene expressions by rat calvarial osteoblasts seeded on these hybrid scaffolds demonstrated remarkable spatiotemporal gene activation. Transcriptional-level gene expressions for alkaline phosphatase (ALP), osteopontin (OPN), bone sialoprotein (BSP), and osteocalcin (OCN) were significantly higher on the hybrid fibrous scaffolds ($p < 0.001$) that were largely dependent on fiber diameter compared. Taken together, our results suggest that PCL/BG fibrous scaffolds may accelerate bone formation by providing a favorable microenvironment.

KEYWORDS: organic-inorganic bioactive hybrid scaffolds, bone regeneration, electrospinning, mechanical properties, osteoblast gene expression
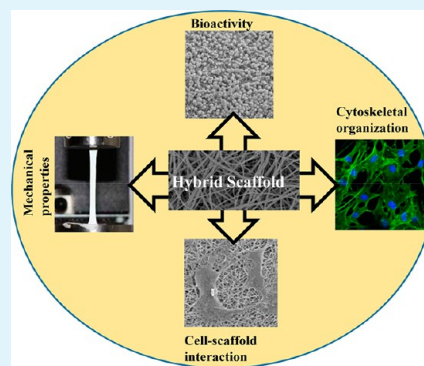
INTRODUCTION

Scaffold-guided bone regeneration holds a promise in providing an improved clinical therapy to repair critical bone defects resulting from disease or trauma.[1] The ultimate goal of scaffold design is to mimic the complex structural composition, spatial distribution, and functionality of native tissues, and to provide a 3D template for cell growth and neo-tissue formation.[2] Therefore, scaffolds for bone regeneration are desired to be mechanically stable, biocompatible, bioactive, osteoconductive, degradable at a rate comparable to neogenesis, and have porous architectures to support bone ingrowth.[2,3] Although fulfilling the above requirements remains a challenge, the nano-composite structure of the bone extracellular matrix (ECM) consisting of collagen fibrils and carbonated hydroxyapatite (HA)-like nanocrystals[4,5] provides a framework for the design of synthetic scaffolds. In an attempt to fabricate scaffolds that mimic the bone ECM using processing techniques such as electrospinning, phase separation, and self-assembly,[6,7] nanoparticles, nanofibers, and nanocomposites have received considerable attention. Previous studies have demonstrated that the high specific surface area and porosity associated with electrospun nanofibrous structures enhanced the osteogenic potential of synthetic scaffolds in terms of protein adsorption,[8] cell adhesion,[9] proliferation, differentiation, and mineralized tissue biosynthesis.[8] It has also been suggested that varying the fiber diameter, the pore size, porosity and surface area of the scaffold could influence their biological performances including cell attachment, proliferation, and differentiation.[10−12]

To make a significant progress towards tissue engineered bone, O/I hybrid scaffolds play an integral part. Notwithstanding this, however, synthetic biodegradable aliphatic polyesters (e.g., PCL) have been among the preferred and most widely studied scaffold materials for bone regeneration because of its good biocompatibility, slow degradation, and good processability.[13,14] Because of the use of PCL scaffolds for bone regeneration led to poor bioactivity and low stiffness,[15,16] various studies attempted to incorporate bioactive inorganic nanoparticles into biodegradable polymers as fillers to form composite nanofibers.[17−19] Although some encouraging results are reported, most of these electrospun composite fibers have two major drawbacks: (1) agglomeration of nanoparticle fillers within the fibrous matrix and, (2) lack of specific interactions between the organic and inorganic phases leading to poor dispersion, compromised mechanical properties, and unfavor-

able cellular responses.[20,21] One of the strategies to overcome this notable problem is the preparation of scaffolds from sol–gel-derived hybrids by the electrospinning process. Previously we reported that tertiary BGs can be homogenously incorporated into PCL using a sol-gel process and demonstrated the feasibility of electrospinning the gelling composition.[22] In that study, the electrospinning parameters were not optimized and the biological evaluations were not carried out.[22] In view of this, one of the objectives of our study was to fabricate and evaluate property-relationships of sol–gel-derived O/I hybrid fibrous scaffolds.

Scaffolds should not only serve as structural templates for cell attachment and viability, but also should guide tissue formation by regulating spatial and temporal bone-associated gene (collagen type I, alkaline phosphatase, osteopontin, bone sialoprotein, and osteocalcin) expressions leading to protein translation and matrix remodeling. Not surprisingly, osteoblast differentiation is a multistep process modulated by an integrated cascade of gene expression that initially supports proliferation and the sequential expression of genes associated with the biosynthesis, organization, and mineralization of the bone ECM.[23] Bone-associated gene and protein expressions of osteoblast and osteoblast-like cells seeded on 3D collagen and biodegradable synthetic scaffolds have been studied.[8,24−26] These studies demonstrated that the 3D topography of the polymeric scaffolds played a role in enhanced bone-associated gene expressions. The role of 3D O/I hybrid fibrous scaffolds on bone-associated gene expression is, however, unknown. We hypothesized that, in addition to the 3D fibrous structures, the homogenously incorporated inorganic component play a significant role in osteogenic gene expression. Furthermore, we tested the hypothesis that in vitro mineralization and cell viability is enhanced on 3D PCL/BG hybrid fibrous scaffolds compared with a previously widely studied PCL.

■ EXPERIMENTAL SECTION

Fabrication of PCL/BG Hybrid Scaffolds. The electrospinning of sol–gel derived PCL/BG hybrids was carried out as described previously;[22] except that instead of a stationary collector, we have utilized a custom designed rotating mandrel collector to produce larger mat size and to control mat morphology. Accordingly, 1 mL of the viscous 1:1 PCL/BG hybrid solution was transferred to a plastic syringe equipped with a 22 gauge stainless steel needle, which was connected to a high voltage supply. The electrospinning parameters were optimized to produce two distinct fiber diameters. For PCL/BG hybrid scaffolds with 260 nm mean fiber diameter: 18 kV (voltage), 0.1 mL/h (flow rate), and 10 cm (needle tip to collector distance (TCD)); for PCL/BG hybrid scaffolds with 600 nm mean fiber diameter: 15 kV (voltage), 0.15 mL/h (flow rate), and 6 cm (TCD) were identified. For fabricating PCL control nanofiber scaffolds, 10 wt % of the polymer solution in 4:1 chloroform/dimethyl sulfoxide ratio was spun at 18 kV (voltage), 0.1 mL/h (flow rate), and 10 cm (TCD). Sample nomenclature is as follows: the hybrid fibrous scaffolds with 600 nm fiber diameter are named as coarse fiber (abbreviated as HC) whereas hybrid fibrous scaffolds with 260 nm fiber diameter are named as fine fiber (abbreviated as HF). The control polycaprolactone fibrous scaffolds are named as PCL.

Scaffold Morphology and Porosity Characterization. The morphologies of PCL/BG hybrids and PCL control fibrous scaffolds were visualized by HITACHI S-3400N Variable Pressure Scanning Electron Microscope (VP-SEM; Hitachi, Japan) at a working distance of 10 mm and an accelerating voltage of 10 keV after sputter coating with gold. Scaffold porosity and pore-size were determined on rectangular (1.5 cm by 3 cm) specimens using Autopore IV mercury porosimeter (Micromeritics, Norcross, GA) according to our pervious publication.[27]

Water Contact Angle (WCA) Measurements. Surface wettability of the electrospun PCL/BG hybrid and PCL fibrous scaffolds was studied by static WCA method at 21 °C. The WCA of different fibrous scaffolds were measured with deionized water using a Kruss DSA 100 goniometer (Hamburg, Germany) followed up by drop shape analysis software. Values were determined by averaging measured data for 5 μL droplets at three different spots on each fibrous scaffold. The Laplace−Young fitting method was used to calculate all the static contact angles.

Mechanical Testing of PCL/BG Hybrid Scaffolds. Mechanical properties of the fibrous scaffolds were determined in tension using an Instron 3345 universal testing machine (Instron, Canton, MA) equipped with a 50 N load cell. Specimens (5 mm width × 30 mm length × ~350 μm thick) were cut from the electrospun PCL/BG hybrids and PCL mats using a sharp blade. For wet condition measurements, prepared specimens were soaked in simulated body fluid (SBF) for 24 h prior to testing. For each group, independent specimens ($n = 5$) were tested at a crosshead speed of 1 mm/min. Stress−strain relationships were obtained from the load and displacement data. The Young's modulus (E) was determined by calculating the slope of the linear portion of the stress−strain curves, which corresponds to a strain of 15−20%. The ultimate tensile strength (UTS), defined as the maximum stress achieved prior to failure, was obtained from the stress−strain curves of each specimen.

In Vitro Bioactivity of PCL/BG Hybrid Fibrous Scaffolds. The in vitro bioactivity of the electrospun PCL/BG hybrid mats was carried out by incubating in SBF.[28] The SBF solution has a composition and concentration close to those of the inorganic constituents of human plasma, and was prepared according to our previous publication.[29] Electrospun PCL/BG hybrid fibrous scaffolds (1.5 cm in diameter and ~350 μm in thickness) were placed in polypropylene vials containing 5 mL SBF and incubated at 37 °C inside an orbital shaker at a constant speed of 120 rpm for 1 and 4 days without SBF refreshing. After each incubation period, the samples were removed from the SBF and rinsed thoroughly with phosphate-buffer saline (PBS), 70% ethanol, and dried overnight at 37 °C.

Sample Preparation and MC3T3-E1 Cell Culture. Electrospun PCL/BG hybrid and PCL control fibrous scaffolds were rinsed with ethanol and dried before sterilizing in low-temperature radio-frequency glow discharge argon plasma using a PDC-32G plasma cleaner (Harrick Plasma, Ithaca, NY) for 4 min. Prior to the seeding of cells, the scaffolds were equilibrated in 1.5 ml of serum-free culture medium in 24 well culture plates. After 24 h, the serum-free medium was removed and newborn mouse calvaria-derived MC3T3-E1 subclone 4 pre-osteoblast cells (ATCC, USA) were seeded at a density of 2.5×10^4 cells/scaffold on PCL/BG hybrids and PCL control fibrous scaffolds. Cells were cultured for up to 7 days in alpha-MEM medium supplemented with 10% fetal bovine serum (FBS; Gibco, Carlsbad, CA), 100 U/mL penicillin and 100 μg/mL streptomycin (Gibco, Carlsbad, CA) in a humidified atmosphere of 95% air/5% CO_2 at 37 °C. The medium was refreshed every 3 days. MC3T3-E1 cell proliferation after 1, 4, and 7 days of culture was determined using the CyQuant cell proliferation assay kit incorporating a nucleic acid binding dye (Molecular Probes, OR) according to the manufacturer's protocol.

Confocal Microscopy and SEM Analysis of MC3T3-E1 Cell Morphology. Following the above prescribed culture times, MC3T3-E1 cells were fixed, stained, and processed for confocal imaging according to our previous published procedures.[27] For SEM imaging, cells were fixed with 4% glutaraldehyde solution (Sigma-Aldrich) for 15 min, rinsed three times with PBS and dehydrated in a graded ethanol (25, 50, 75, 90, 95, and 100%) for 5 min at each concentration. Samples were then subsequently incubated in 25/75, 50/50, 75/25, 0/100% hexamethyldisilazane (HMDS; Sigma-Aldrich) for 10 min to preserve osteoblast morphology and dried in air. Surface morphology of samples were examined using Hitachi 3400-N VP-SEM.

Osteoblast Differentiation and Bone-Associated Gene Expression Studies. *Osteoblast Isolation and Culture.* Rat calvarial osteoblasts (RCO) were isolated from 0- to 5-day-old neonatal Sprague Dawley rats. All animal procedures were approved by the

Council on Animal Care of the University of Western Ontario and were in accordance with the guidelines of the Canadian Council on Animal Care. Briefly, the parietal and occipital bones were dissected and washed with phosphate-buffered saline (PBS). The harvested bones were minced and subsequently digested by incubation in 700 U/ml of type I collagenase (Sigma-Aldrich, St. Louis, MO) at 37 °C. The supernatant of the first digestion was discarded and the calvarial fragments were treated five more times with collagenase (20 min at 37 °C), and the subsequent supernatants were collected, combined together, and sedimented. The resulting cell pellet was resuspended and cultured in α minimum essential media (α-MEM) supplemented with 10% (v/v) fetal bovine serum (FBS; Life Technologies Inc., Carlsbad, CA), antibiotics and antimycotic (AA; 200 U/mL penicillin, 200 μg/mL streptomycin, 0.5 μg/mL amphotericin B) (Gibco, Carlsbad, CA). Primary RCO cultures were maintained in a humidified 5% CO_2 atmosphere at 37 °C and expanded until confluent and released from 75-cm^2 tissue culture plastic flasks using a 0.05% trypsin and 0.2 g/L EDTA solution, and cell number was determined by using a hemocytometer. For alkaline phosphatase enzyme (ALP) activity assay and gene expression experiments, RCOs (primary or passage 1) were seeded on sterilized and plasma cleaned PCL/BG hybrid and PCL control scaffolds in 24-well plates at a density of 1×10^5 cell/scaffold and cultured in α-MEM (supplemented with 10% FBS and AA) for 3 days. Subsequently, RCO's were cultured in osteogenic medium (regular medium described above supplemented with 2 mM β-glycerophosphate and 50 μg/mL ascorbic acid) and incubated for an additional 7 or 14 days (with medium changed every 2−3 days).

ALP Activity Measurement. ALP activity was measured using a commercially available SensoLyte *p*-nitrophenol phosphate (pNPP) alkaline phosphatase assay kit (AnaSpec, CA) according to the manufacturer's instructions following 0, 7, and 14 days of culture time. Bicinchoninic acid (BCA) protein assay kit (Thermo Fisher Scientific, Waltham, MA) was used to quantify total intracellular protein content as per supplier's instructions. The results of ALP activity were reported as ng of p-nitrophenol produced per hour, normalized to total protein content (ng/h/mg protein). Four electrospun PCL/BG and PCL control fibrous scaffolds were used in each experiment and was repeated twice ($n = 8$).

Quantitative Assessment of Osteoblast Marker Gene Expression. Total RNA was extracted using TRIzol (Invitrogen) prior to the addition of osteogenic medium (days 0), and at days 7 and 14 after the addition. RNA was purified using an RNeasy Micro Kit (Qiagen - Canada, Toronto, ON) and genomic DNA removed using DNase I (Qiagen), according to the manufacturer's instructions. The total RNA concentration and purity was determined from the absorbance at 260 and 280 nm using a Nanodrop spectrophotometer (Thermo Fisher Scientific, Waltham, MA, USA). Complementary DNA (cDNA) was synthesized using 1 μg of total RNA primed with oligo(dT)$_{12-18}$ as described in SuperScript (Table 1). Quantitative real-time PCR was conducted in 10 μl reaction volumes, using a Chromo4 Real-time Thermal Cycler (Bio-Rad, Mississauga, Canada) and gene expressions of type I collagen (Col 1), tissue non-specific alkaline phosphatase (ALP), osteopontin (OPN), bone sialoprotein (BSP), osteocalcin (OCN) and GAPDH were then determined with iQ SYBR Green Supermix (Bio-Rad) according to the recommended protocol of the manufacturer. Cycling parameters were as follows:[30] denaturation 95 °C (15 s), gradient annealing 53 °C/58 °C (60 s), extension 72 °C (30 s), and running for 40 cycles. mRNA expression in RCOs was normalized to GAPDH with at least three repeats per experimental group and expressed as a relative ratio using the Gene Expression Macro analysis software (Bio-Rad, Mississauga, Canada). Although clonal murine calvarial MC3T3-E1 cells are the predominant in vitro model for studying bone cell interactions with biomaterials, osteoblast differentiation, and ECM signaling we specifically chose primary RCO cells for bone-associated gene expression studies since our long-term objective is to implant the tissue-engineered bone construct into animal models. We believe that this is a logical approach as the use of cell lines to engineer a tissue for eventual in vivo studies is obviously undesirable.

Table 1. Primers for Rat-Specific Osteoblast mRNA Amplification

gene	primer sequence
alkaline phosphatase (ALP)	forward: 5′-AGGCAGGATTGACCACGG-3′
	reverse: 5′-TGTAGTTCTGCTCATGGA-3′
collagen, α 1, Type 1 collagen	forward: 5′-CAACAAATCCCCACACAC-3′
	reverse: 5′-CACACAAAGACAAGAACGAG-3′
osteocalcin (OCN)	forward: 5′-CTGCATTCTGCCTCTCTGAC-3′
	reverse: 5′CTATTCACCACCTTACTGCCC-3′
osteopontin (OPN)	forward: 5′-GTTTGCCTTTGCCTGTTC-3′
	reverse: 5′-ATCGTCGTCGTCATCATC-3′
bone sialoprotein (BSP)	forward: 5′-CTGCTTTAATCTTGCTCTG-3′
	reverse: 5′-CCATCTCCATTTTCTTCC-3′
GAPDH	forward: 5′-GGTGGTCTCCTCTGACTTCAACA-3′
	reverse: 5′-GTTGCTGTAGCCAAATTCGTTGT-3′

Statistical Analyses. All statistical analyses were performed using Instat 3.0 (GraphPad Software, Inc., San Diego, CA). One- and two-way analyses of variance (ANOVA) and a Tukey−Kramer multiple comparisons test were used to assess the statistical significance of the data at $p < 0.05$.

■ RESULTS

Morphology, Fiber-Size Distribution, and Porosity of PCL/BG Hybrid Fibrous Scaffolds. In this study, biomimetic and homogeneous 3D O/I hybrid fibrous scaffolds consisting of 50 wt % PCL and 50 wt % tertiary BG were successfully fabricated by a combined sol-gel and electrospinning processes to exploit the synergetic effect of PCL and BG when combined at a molecular level. The choice of this ratio was based on our previous finding that this composition led to the best spatially distributed inorganic components in the O/I hybrid system from sol−gel reactions.[22] It can be seen from Figure 1A−C that the sol−gel-derived PCL/BG hybrid and PCL control fibrous scaffolds had randomly oriented fibers forming a porous 3D structure and are reasonably uniform in sizes with no beading, fusion or bundling effects. The SEM micrographs were further analyzed to determine the fiber diameter distribution whereby individual fiber diameters ($n = 100$) at six random locations in the mats were measured from representative SEM images by using ImageJ software. The histograms corresponding to the SEM images displayed in Figure 1 showed that the PCL/BG hybrid and PCL fibrous scaffolds had unimodal distributions and correlated well with a Gaussian nonlinear fit. Accordingly, two different PCL/BG hybrid scaffolds with fiber diameter distributions of 260 ± 60 nm (HF) and 600 ± 166 nm (HC) were fabricated. The control PCL scaffold had 300 ± 80 nm fiber diameter which was not statistically different from the HF hybrid scaffolds (p > 0.05), allowing us to evaluate composition effects. Tissue engineering scaffolds are expected to have high porosity and interconnected pore structures for enhancing cellular infiltration, nutrient and metabolic transport, and matrix remodeling. We therefore examined the effect of fiber diameter on the porosity of PCL/BG hybrid scaffolds. Pore-size distribution and pore parameters of electrospun PCL/BG hybrid scaffolds determined by a mercury porosimetry are presented in Figure 1D and Table 2. From Figure 1D, the mean pore diameter for HF hybrid scaffolds was 33 μm; however, the HC scaffold exhibited a bimodal pore diameter distribution,

7576

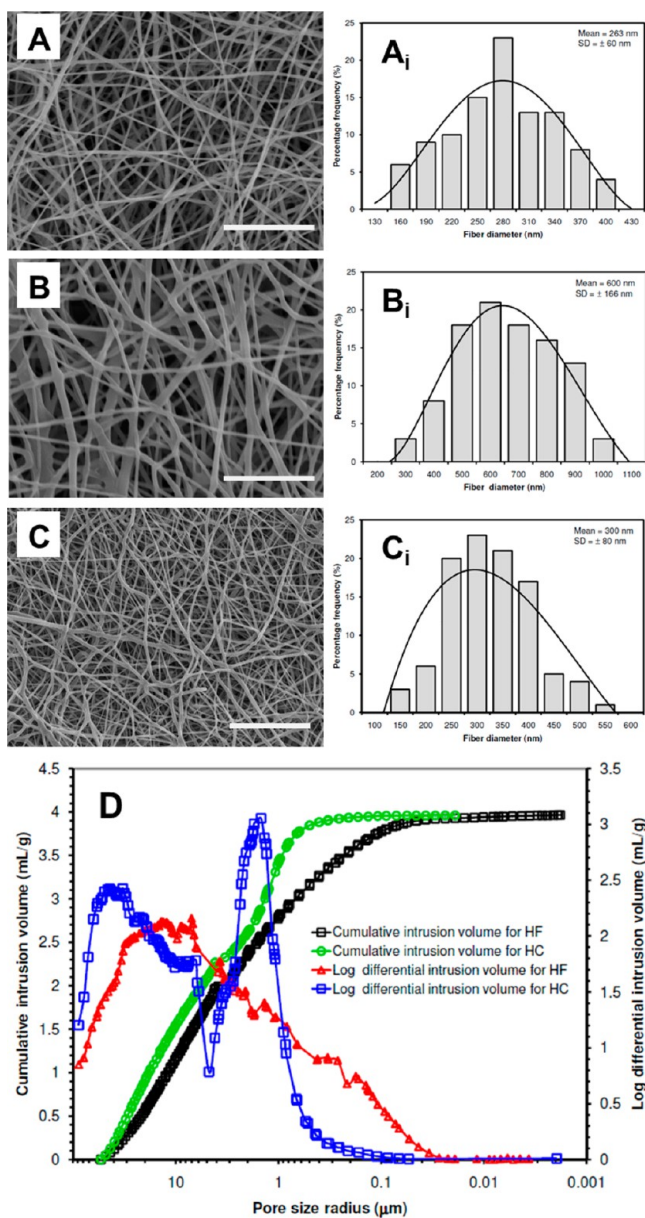dx.doi.org/10.1021/am401861w | *ACS Appl. Mater. Interfaces* 2013, 5, 7574−7583

Figure 1. Representative SEM micrographs, fiber diameter, and pore-size distribution plots for PCL/BG hybrid and PCL fibrous scaffolds. The fiber diameter distribution plots were generated from six random SEM micrographs (n = 100) acquired at random locations, and ImageJ software was used to measure individual fiber diameters. Pore-size distributions are plotted as a function of both differential and cumulative intrusion volumes. (A) PCL/BG hybrid scaffold with 263 ± 60 nm fiber diameter (HF), (B) PCL/BG hybrid scaffold with 600 ± 166 nm fiber diameter (HC), (C) PCL scaffold with 300 ± 80 nm fiber diameter, and (D) effect of fiber diameter on pore-size distribution of HF and HC scaffolds. Scale bar represents 10 μm.

with one major peak at 52 μm and a minor secondary peak at 3 μm. Scaffold compression during the mercury intrusion and extrusion cycles was minimal suggesting the reliability of the porosity and pore-size results obtained.[27] Porosity analyses of HF and HC electrospun hybrid scaffolds revealed 76.54% and 83.23%, respectively (Table 2), suggesting the utility of these scaffolds for bone tissue engineering applications. Please note that additional parameters are included in Table 2 as they are needed to calculate porosity and average pore size.

Table 2. Mercury Intrusion Porosimetry (MIP) Analysis Data for the Electrospun PCL/BG Hybrid Fibrous Scaffolds

attributes	HF	HC
total intrusion volume (mL/g)	3.89	3.94
penetrometer weight m_p (g)	62.24	62.24
assembly weight m_a (g)	143.45[a]	143.45[a]
	138.43[b]	133.65[b]
sample weight (m_s) (g)	0.08	0.16
sample bulk volume (V_b) (mL)	0.41	0.76
porosity (%)	76.54	83.23
average pore diameter (μm)	33.06	51.52[c]
		2.98[d]

[a]Assembly weight without sample: $m_a = m_p + m_{Hg}$, where m_{Hg} is the weight of mercury. [b]Assembly weight with sample: $m_a = m_p + m_{Hg} + m_s$ [c]First peak (large pore size region) of the bimodal distribution. [d]Second peak (small pore size region) of the bimodal distribution.

Surface Wettability of PCL/BG Hybrid Fibrous scaffolds. Given that the current hybrid scaffolds were fabricated with two distinctive fiber diameters, we expected that the wetting properties to be affected by both composition (hybrid vs. PCL) and fiber diameter (HC vs. HF). The water sessile drop deformation and contact angle data with respect to time are presented in Figure 2, from which it can be inferred that the
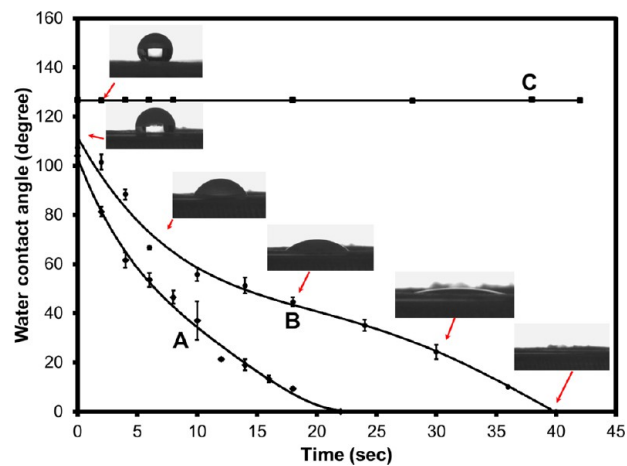

Figure 2. Water contact angle (WCA) measurements of electrospun PCL/BG hybrids and PCL control fibrous scaffolds. Representative time-frame images of water sessile drop on PCL/BG hybrid and PCL fibrous scaffolds and WCAs as a function of time for electrospun (A) HC scaffolds, (B) HF scaffolds, and (C) PCL scaffolds. Error bars represent means ± SD for n = 3.

water droplet maintained its round shape on the control electrospun PCL scaffolds (Figure 2C) and its WCA was found to be 126.3 ± 1.6° during a 45 s observation. To the contrary, the water sessile droplets deformed quickly and spread on the surface of the electrospun PCL/BG hybrid scaffolds, and penetrated into the scaffold meshwork at the end of a 45 s observation. Furthermore, the WCA measurements with respect to exposure time demonstrated that the spreading velocity of water droplets on HC fibrous scaffolds was higher than HF fibrous scaffolds (Figure 2A, B). The time for the spreading of 5 μL of water sessile droplet on the scaffolds was 40 s on HF and 22 s on HC.

Mechanical Properties and In Vitro Mineralization of PCL/BG Hybrid Fibrous Scaffolds. In a previous study,[29] we
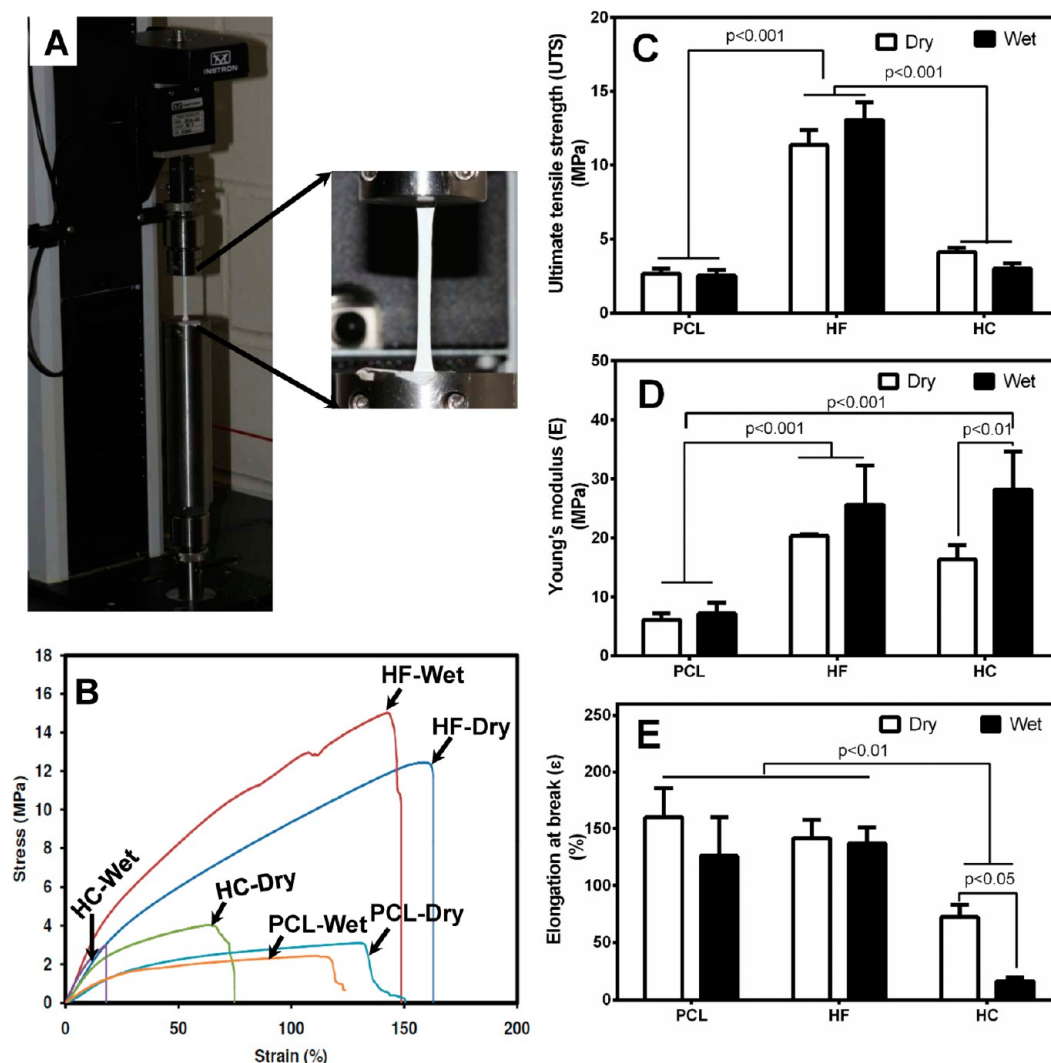
Figure 3. Tensile mechanical properties for PCL/BG hybrid and PCL control fibrous scaffolds. (A) Tensile test set-up; (B) representative stress–strain curves; (C) ultimate tensile strength (UTS); (D) Young's moduli (*E*), and (E) elongation at break (*ε*) of PCL/BG hybrids and PCL control fibrous scaffolds measured in dry and wet testing condition. The wet condition measurement was taken after soaking in SBF for 24 h. Data are mean ± SD (*n* = 5). Statistical analysis of the data were conducted using two-way ANOVA and Tukey–Kramer multiple comparative test, *p* < 0.05.

have reported the composition-dependent mechanical properties of PCL/BG hybrid monoliths (solid cylindrical discs). These solid discs, however, cannot be used as tissue engineering scaffolds because of their 2D surfaces. Because mechanical properties of the PCL/BG hybrid nanofibrous scaffolds were important design considerations in this study, we investigated the tensile properties of the 3D fibrous scaffolds and the data are collectively presented in Figure 3.

As can be seen from representative stress–strain curves (Figure 3B) both the fiber diameter of the PCL/BG hybrid fibrous scaffolds and the test condition (dry or wet) influenced their mechanical properties. HF fibrous scaffolds had significantly higher UTS in both dry and wet testing conditions than both HC fibrous scaffolds and the PCL controls (Figure 3C; p < 0.001). Within the three different scaffolds, the testing condition did not have a significant effect on the UTS (*p* > 0.05). Both HC and HF fibrous scaffolds showed significantly higher modulus (a measure of stiffness) compared with PCL controls (Figure 3D; p < 0.001). Whereas the testing condition had no significant effect on the modulus values for the control PCL fibrous scaffolds, it had a significant effect on the hybrid

fibrous scaffolds whereby the wet condition increased the modulus. This finding is attributed to the plasticizing effect of the soaking solution and is consistent with the WCA data (Figure 2) that showed enhanced wetting for the hybrid fibrous scaffolds. Finally, the HC fibrous scaffold had significantly lower elongation at break than both HF and PCL control scaffolds (Figure 3E; p < 0.01). Furthermore, it is evident that the wetted HC scaffolds had significantly diminished elongation at break (p < 0.05). Although the test condition has a strong effect on the toughness (area under the stress–strain curve) for HC scaffolds, it had a minimal influence on HF and PCL control scaffolds. Collectively, these data strongly suggest that the overall mechanical properties of the PCL/BG hybrid fibrous scaffolds are superior as compared to PCL, which is the dominantly used fibrous scaffold for bone tissue engineering.[31,32] It is also evident that the HF scaffolds had higher tensile strength than HC scaffolds because of its smaller average pore diameter, Table 2. Given its attractive mechanical properties, we tested the bioactivity of HF scaffolds and compared it to PCL controls. As shown in Figure 4, HF scaffolds were covered with heterogeneous and sparsely
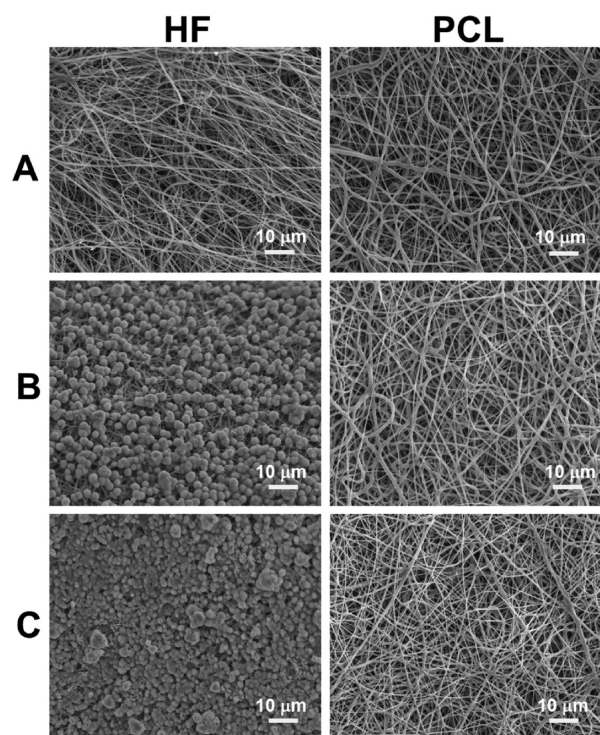
Figure 4. Representative SEM micrographs showing the evolution of HA deposit on electrospun PCL/BG hybrids and PCL control fibrous scaffold surfaces after incubating in SBF at different time points. (A) Scaffolds before incubation starts; (B, C) scaffolds after incubating in SBF for 24 and 96 h, respectively.

dispersed spherically-shaped particles after 24 h of incubation in SBF (Figure 4B), which became denser at longer incubation times.[29] Conversely, no apatite deposition was observed on the PCL control scaffolds.

MC3T3-E1 Cell Spreading and Proliferation on PCL/BG Hybrid Fibrous Scaffolds. Favorable cell attachment and spreading on scaffolds is an important requirement for subsequent cellular activities. MC3T3-E1 cell interactions data with the electrospun PCL/BG hybrid fibrous scaffolds at 1, 4, and 7 days are collectively shown in Figure 5. At day 1, on PCL/BG hybrid and PCL control scaffolds, cells spread well and were in intimate contact with the scaffold surfaces. At day 4 and 7, cells were observed with enhanced cytoplasmic extensions, suggesting favorable cell−scaffold interactions. The proliferation of MC3T3-E1 cells on the PCL/BG hybrid fibrous scaffolds and the PCL control at different time points demonstrating MC3T3-E1 cell growth for up to 7 days of culture is shown in Figure 5D. There was no significant difference in cell number between all scaffolds at day 1 ($p > 0.05$). Similarly, there was no significant difference in cell number between HC and PCL scaffolds at days 4 and 7 ($p > 0.05$). However, HF fibrous scaffolds promoted cell growth significantly at days 4 and 7 ($p < 0.05$).

ALP Activity and Bone-Associated Gene Expression. ALP is an enzyme routinely used as an early marker for osteoblasts differentiation and plays a critical role in regulating mineralization of the extracellular matrix.[33] Given its importance, the ALP activity of RCO cells on PCL/BG hybrid scaffolds was assessed by a colorimetric method. This was achieved by seeding RCOs on HF, HC, and PCL fibrous scaffolds and cultured for 3 days. Medium was then supplemented with β-glycerophosphate and ascorbic acid to
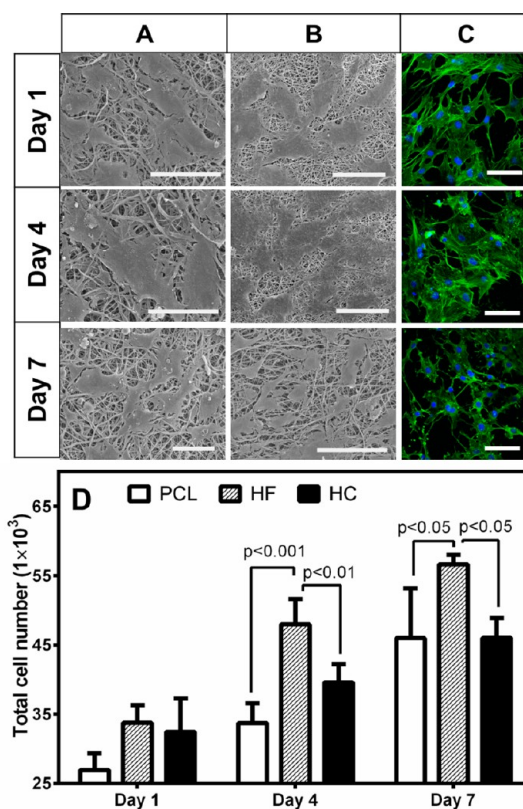

Figure 5. MC3T3-E1 cell morphology and proliferation on electrospun PCL/BG and PCL control fibrous scaffolds. MC3T3-E1 cells at 2.5×10^4 cells/scaffold were seeded on electrospun PCL/BG hybrids and PCL control. Osteoblast morphology on the scaffold surface was obtained by confocal microscopy and SEM after 1, 4, and 7 days of culture. (A, B) Representative SEM micrographs of MC3T3-E1 cells on HC and HF scaffolds respectively; (C) Confocal micrographs of MC3T3-E1 cells on HF scaffolds (green = F-actin and blue = nuclei); (D) Cell proliferation per scaffold as determined by CyQUANT fluorescent assay protocol after day 1, 4, and 7 of cultures. Scale bar for A−C represents 40 μm. Data are the mean ± SEM ($n = 5$). Statistical analysis of the data at each time point were conducted separately using one-way ANOVA and Tukey−Kramer multiple comparative test, $p < 0.05$.

induce osteoblastic differentiation (day 0) and cells were cultured for an additional 7 and 14 days. As shown in Figure 6A, ALP activity of RCO cultured on HF and HC fibrous scaffolds was significantly higher than the PCL control for day 0 ($p < 0.01$). No significant differences on ALP activities were observed in all scaffolds on day 7 ($p > 0.05$). Between days 7 and 14, ALP activity of RCO cells cultured on HF and HC were significantly higher than the PCL control scaffold ($p < 0.01$ for HC and $p < 0.001$ for HF). Furthermore, a significantly higher ALP activity ($p < 0.05$) was observed for HF scaffolds compared to HC scaffolds. These results indicate that the PCL/BG hybrid scaffolds promoted ALP activity by RCO cells, which is a strong marker of osteoblasts phenotype and mineralization.[34] To further evaluate osteogenic differentiation on electrospun PCL/BG hybrid and PCL fibrous scaffolds, we performed quantitative real-time PCR measurements. The expression of ALP, Col 1, OPN, BSP, and OCN were determined using primers (Table 1) specific for each osteogenic marker gene and were normalized to GAPDH and expressed as fold changes relative to the gene expression at day 0 of the PCL control (Figure 6B−F). Consistent with the
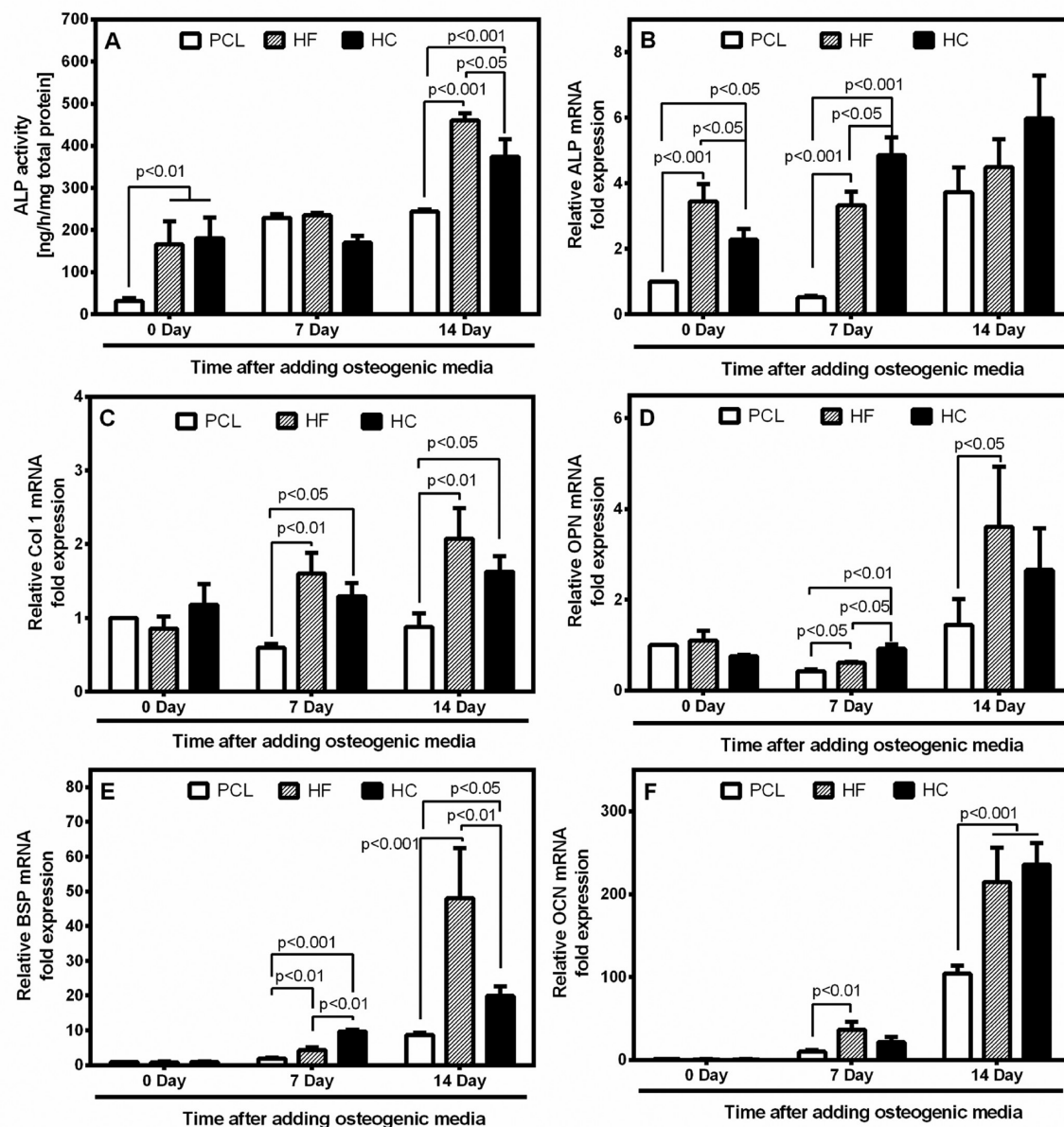
Figure 6. Alkaline phosphatase (ALP) enzyme activity assay and gene expression of bone-associated mRNAs by primary osteoblasts grown on PCL/BG hybrid and pure PCL (control) fibrous scaffolds. RCOs were seeded on HF, HC and PCL fibrous scaffolds and cultured for 3 days. Medium was then supplemented with β-glycerophosphate and ascorbic acid to induce osteoblastic differentiation (day 0) and cells were cultured for an additional 7 and 14 days. (A) ALP activity quantification, and (B–F) Spatiotemporal expressions of ALP, type I collagen (Col 1), osteopontin (OPN), bone sialoprotein (BSP), and osteocalcin (OC) mRNAs by qRT-PCR. The mRNA levels of the genes of interest were normalised against the expression of GAPDH, and are presented as fold changes relative to PCL at day 0. The bars represent mean ± SEM for two independent experiments and four scaffolds in each experiment for ALP activity ($n = 8$) and triplicate samples from three independent experiments for gene expressions ($n = 3$). Statistical analysis of the data at each time point were conducted separately using one-way ANOVA and Tukey–Kramer multiple comparative test, $p < 0.05$.

enzyme activity data (Figure 6A), RCO cells cultured on HF and HC scaffolds expressed significantly higher ALP compared with the PCL control following days 0 and 7 cultures in osteogenic media (Figure 6B; $p < 0.05$). Between HF and HC, there was a significantly higher ALP gene expression on HF scaffolds at early culture time (day 0) ($p < 0.05$), and on HC scaffolds at day 7. After 14 days of culture, ALP gene expression increased modestly but not significantly in HF and HC hybrid scaffolds in comparison to day 7 ($p > 0.05$). The expression of Col 1 on the HF and HC scaffolds increased significantly for 7

and 14 days of cultures compared with the PCL control ($p < 0.05$). While Col 1 gene expression by RCO cells seeded on HF and HC hybrid scaffolds showed an upward trend with culture time, its expression on PCL control scaffolds decreased on day 7 (0.87-fold) then slightly increased on day 14 (1.2-fold). Unlike ALP and Col 1 gene expressions, OPN, BSP, and OCN gene expressions were significantly delayed until 14 days of culture (Figure 6 D–F). Furthermore, while both HF and HC scaffolds up-regulated OCN gene expression significantly at day 14 ($p < 0.001$), OPN and BSP were significantly up-regulated

7580

dx.doi.org/10.1021/am401861w | ACS Appl. Mater. Interfaces 2013, 5, 7574–7583

only by cells cultured on HF scaffolds compared with the PCL control ($p < 0.05$ and $p < 0.001$, respectively) suggesting a spatiotemporal regulation of gene expression.

DISCUSSION

This study demonstrates the potential application of novel sol–gel-derived and electrospun PCL/BG hybrid fibrous scaffolds and the effect of fiber diameter on both scaffold properties and cellular responses for bone regeneration. Although the combination of BG nanoparticles or nanofibers with polymeric systems enables the production of nanocomposites as scaffolds for bone tissue engineering (reviewed in detail in ref 35), sol–gel hybridization of the polymer with the inorganic glass components at a molecular scale is a new enabling strategy.[22] In this strategy, the inorganic components are strongly hydrogen bonded with the polymer matrix, creating a homogenous material that can be electrospun into fibrous scaffolds before the network crosslinks. Our data (Figure 1 and Table 2) demonstrated that the electrospun PCL/BG hybrid scaffolds with 260 nm average fiber diameter (fine fiber diameter; HF) and 600 nm fiber diameter (coarse fiber diameter; HC) yielded an average pore size of 33 and 52 μm, respectively. Furthermore, the porosity of HF and HC scaffolds was 77 and 83%, respectively. We believe that the lower total pore volume and porosity observed in the HF scaffolds resulted from the denser structure formed by the lower fiber diameter. The three important parameters that play a considerable role in the functional and mechanical performance of electrospun fibrous scaffolds are fiber diameter, interconnected pore size, and percentage porosity; as these influence cell infiltration and the transport of oxygen and nutrients to the cells and removal of waste products.[36] Smaller fiber diameters (<1 μm), pore-sizes in excess of the size of the cell (>20 μm), and porosities in excess of 70% are deemed to be requirements for electrospun scaffolds.[37] Oftentimes, one parameter is optimized at the expense of the other and even the application of ultrasonic methods and sacrificial polymers did not appear to optimize all of the above parameters.[37,38] Pore size and porosity are particularly problematic to optimize in electrospun BG scaffolds.[22,39] By combining sol–gel chemistry and electrospinning in situ, our study indicated that all the required scaffold parameters were within the desired ranges. The wettability of scaffolds is another useful parameter that influences cell adhesion and spreading and determines subsequent processes such as cell morphology, proliferation, and differentiation.[40,41] Osteogenic cells tend to prefer hydrophilic surfaces rather than hydrophobic surfaces.[42] Results from WCA study (Figure 2) of the electrospun PCL/BG hybrids and PCL fibrous scaffolds revealed that the wetting was governed by both the composition and the fiber diameter. It is known that fibrous scaffolds fabricated from a given material will have a higher WCA than the film counterpart because of the rough surface topography of electrospun fibers compared with relatively smooth topography observed in films.[43] It was not, therefore, surprising that we observed higher WCA for the electrospun PCL fibrous scaffold (126°) than the 76° WCA value we measured for PCL films. Consequently, the test water droplet could not easily penetrate into inter-fiber pores on the rough surface of hydrophobic fibrous scaffolds. Thus, the water droplet was supported by a semi-solid and semi-air plane surface, resulting in a significant increase in the water contact angle.[43,44] In contrary to this, the hybrid fibrous scaffolds fabricated in this study showed a reduced WCA, thus improving

the scaffold wettability.[45] Given that the PCL average fiber diameter was within a comparable range to the HF fibrous scaffolds, the reduced WCA or the higher wettability observed on the PCL/BG fibrous hybrids is mainly contributed from the hydrophilic surface of the BG phase in the hybrid system.[22]

The electrospun PCL/BG hybrid scaffolds in the present study showed significantly higher stiffness ($p < 0.001$) compared to the pure PCL scaffolds owing to the strong hydrogen bonding at molecular scale and homogeneously distributed inorganic network within the PCL matrix.[22] Recent studies showed that electrospun scaffolds filled with more than 25% bioceramic nanoparticles resulted in weakened scaffolds compared to PCL control[18,46] suggesting poor dispersion and absence of interfacial bonding between the nanoparticles and the PCL matrix. Since the current hybrid fibrous scaffolds were prepared with 1:1 ratio of tertiary BG and PCL, it is noteworthy that the observed higher mechanical strength was the consequence of homogeneous distribution. Although data on the effect of fiber diameter on the mechanical properties of electrospun BG/polymer hybrid scaffolds have not been reported in the literature, few studies have shown conflicting results where fiber diameter both increased[47] and decreased[48] the mechanical properties of polymeric fibers. Given that tissue engineering scaffolds are to be used in contact with biological fluids, the wet condition mechanical properties performed after soaking in SBF for 24 h to simulate the effect of physiologic environment revealed that the PCL/BG hybrid scaffolds showed relatively higher moduli as compared to their dry counterparts. Despite the increase in stiffness, the wet condition did not change the UTS significantly. Conversely, no significant difference in stiffness and UTS were observed for PCL control during the dry and wet condition measurements ($p > 0.05$). Both UTS and modulus values for the electrospun control PCL scaffolds were consistent with a recent report by Khademhosseini and co-workers.[49] These findings elucidate that HA precipitation on PCL/BG hybrid scaffold surfaces after 24 h of SBF soaking (Figure 4) might have enhanced the stiffness.[50,51] Notwithstanding a number of reports about sol–gel-derived BG fibers, the most relevant work to the current study dealing with combined sol–gel and electrospinning techniques to fabricate hybrid fibrous scaffolds was conducted by Gao and co-workers who prepared BG/gelatin hybrid fibrous scaffolds.[52] In this cited study, $CaNO_3$ which is presumed to be cytotoxic[53] was used as calcium precursor. In fact, the presence of $CaNO_3$ is one of the reasons why sol–gel-derived electrospun BG fibers in previous studies had to be heated to 600 °C to remove the nitrate which also burns off the polymer, necessitating the re-suspension of BG fibers into a different polymer than the one used in the sol–gel step.[35] Furthermore, swelling, flattening, and fusion of the gelatin matrix even after crosslinking was evident leading to weak hybrid scaffold material (~4.3 MPa of tensile strength). Our study utilized $CaCl_2$ as a calcium precursor that did not require heat treatment and a biocompatible and biodegradable PCL matrix that did not swell and flatten while significantly improving both the mechanical and wetting properties of the scaffolds.

In addition to providing the structural template, bone tissue engineering scaffolds should provide the 3D microenvironment that direct osteoblastic differentiation and tissue maturation. Consistent with previous studies on carbon nanofiber[54] and on PCL fibers,[55] MC3T3-E1 cells seeded on all PCL/BG hybrid scaffolds attached, well-spread, and proliferated in a fiber diameter dependent manner (Figure 5). Some possible reasons

7581

dx.doi.org/10.1021/am401861w | ACS Appl. Mater. Interfaces 2013, 5, 7574–7583

for high cell proliferation on the smaller fiber diameter hybrid scaffolds are large surface area-to-volume ratio for growth factors binding and the pliability of the smaller diameter fibers. Osteoblast differentiation and subsequent bone formation is a gradual and well-orchestrated process associated with characteristic temporal modifications in gene expression and comprised of three developmental stages: (i) proliferation, (ii) extracellular matrix production and maturation, and (iii) matrix mineralization.[56,57] In this three-stage paradigm, Col 1 is expressed during the initial period of proliferation and ECM biosynthesis, whereas ALP which is regarded as characteristic feature of osteoblasts during bone mineralization[58] is expressed during the post proliferative period of ECM maturation, and the expression of OPN, OCN, and BSP occurs later during the third period of matrix mineralization.[59,60] In the present investigation, RCOs on PCL/BG fibrous scaffolds had significantly higher ALP activity on early stage and continued until day 14 (Figure 6A) because of the presence of the tertiary BG component in the hybrid system. Notwithstanding the significant difference that exists in ALP gene expression between the two hybrid fibrous scaffolds for the first 7 days of culture, the corresponding ALP activity was not significant suggesting temporal effects in protein translation. In the ordered hierarchical sequence of events occurring during osteoblast differentiation and matrix mineralization, Col 1 biosynthesis and ALP activity are followed by the deposition of osteoblasts-specific non-collagenous matrix proteins, such as OPN, BSP, and OCN.[23,56,57] In particular, expression of OPN indicates the initial growth of hydroxyapatite crystals and their ability to bind and potentially catalyze mineralization processes.[61,62] The high BSP gene expression suggests copious formation of non-collagenous proteins, promoting efficient nucleation of mineral phases;[63] whereas high expression of OCN gene suggests the formation of a bone-associated protein.[26] In the present study, bone-associated gene expressions were up-regulated throughout the 14 days of culture for PCL/BG hybrid scaffolds as compared to the PCL control. Particularly, the PCL/BG hybrid scaffolds with smaller fiber diameter favored significantly higher gene expression of OPN, BSP and OCN on day 14. Taken together, the current study demonstrated that PCL/BG hybrid scaffolds significantly improved tensile properties, in vitro bioactivity and increased bone-associated gene expression when compared to the commonly used PCL scaffolds and that these gene expressions were up-regulated by the topography of smaller diameter fibers.

CONCLUSIONS

In this study, we investigated the role of a new class of bioactive 3D hybrid fibrous scaffolds on mechanical behavior and spatiotemporal osteoblast gene expression. We demonstrated that highly porous sol-gel derived PCL/BG hybrid fibrous scaffolds with two distinct fiber diameters were fabricated for bone tissue engineering application. A significantly higher tensile strength ($p < 0.001$) was found for the lower fiber diameter PCL/BG hybrid scaffolds as compared to the other scaffolds. Incubation of hybrid scaffolds in SBF resulted in the formation of bonelike apatite on the surface of the PCL/BG fibrous scaffold within 24 h. The PCL/BG hybrid scaffolds supported an earlier and enhanced osteoblast phenotype including proliferation, alkaline phosphatase activity, and changes in genes associated with the osteoblast phenotype. The findings of this study demonstrated that the PCL/BG fibrous scaffolds with a controlled fiber diameter may serve as superior scaffolds versus PCL fibrous scaffolds for promoting bone formation.

AUTHOR INFORMATION

Corresponding Author
*E-mail: kmequani@uwo.ca or arizkall@uwo.ca. Tel: +1 (519) 661-2111, ext. 88573 or 86086. Fax: + 1(519) 661-3498.

Notes
The authors declare no competing financial interest.

REFERENCES

(1) Frohlich, M.; Grayson, W. L.; Wan, L. Q.; Marolt, D.; Drobnic, M.; Vunjak-Novakovic, G. Curr. Stem Cell Res. Ther. 2008, 3, 254−264.
(2) Szpalski, C.; Wetterau, M.; Barr, J.; Warren, S. M. Tissue Eng., Part B 2012, 18, 246−257.
(3) Hutmacher, D. W. Biomaterials 2000, 21, 2529−2543.
(4) Weiner, S.; Wagner, H. D. Annu. Rev Mater. Sci. 1998, 28 (1), 271−298.
(5) Barrere, F.; van Blitterswijk, C. A.; de Groot, K. Int. J. Nanomed. 2006, 1, 317−332.
(6) Allo, B. A.; Costa, D. O.; Dixon, S. J.; Mequanint, K.; Rizkalla, A. S. J. Funct. Biomater. 2012, 3, 432−463.
(7) Holzwarth, J. M.; Ma, P. X. Biomaterials 2011, 32, 9622−9629.
(8) Woo, K. M.; Jun, J. H.; Chen, V. J.; Seo, J.; Baek, J. H.; Ryoo, H. M.; Kim, G. S.; Somerman, M. J.; Ma, P. X. Biomaterials 2007, 28, 335−343.
(9) Saranya, N.; Saravanan, S.; Moorthi, A.; Ramyakrishna, B.; Selvamurugan, N. J. Biomed. Nanotechnol. 2011, 7, 238−244.
(10) Badami, A. S.; Kreke, M. R.; Thompson, M. S.; Riffle, J. S.; Goldstein, A. S. Biomaterials 2006, 27, 596−606.
(11) Sisson, K.; Zhang, C.; Farach-Carson, M. C.; Chase, D. B.; Rabolt, J. F. J. Biomed. Mater. Res A 2010, 94, 1312−1320.
(12) Takahashi, Y.; Tabata, Y. J Biomater. Sci. Polym. Ed. 2004, 15, 41−57.
(13) Cipitria, A.; Skelton, A.; Dargaville, T. R.; Dalton, P. D.; Hutmacher, D. W. J. Mater. Chem. 2011, 21, 9419−9453.
(14) Shin, M.; Yoshimoto, H.; Vacanti, J. P. Tissue Eng. 2004, 10, 33−41.
(15) Taylor, M. S.; Daniels, A. U.; Andriano, K. P.; Heller, J. J. Appl. Biomater. 1994, 5, 151−157.
(16) Lee, S. J.; Oh, S. H.; Liu, J.; Soker, S.; Atala, A.; Yoo, J. J. Biomaterials 2008, 29, 1422−1430.
(17) Ganesh, N.; Jayakumar, R.; Koyakutty, M.; Mony, U.; Nair, S. V. Tissue Eng., Part A 2012, 18, 1867−1881.
(18) Yang, F.; Both, S. K.; Yang, X.; Walboomers, X. F.; Jansen, J. A. Acta Biomater. 2009, 5, 3295−3304.
(19) Patlolla, A.; Collins, G.; Arinzeh, T. L. Acta Biomater. 2010, 6, 90−101.
(20) Song, J. H.; Kim, H. E.; Kim, H. W. J. Biomed. Mater. Res. B: Appl. Biomater. 2007, 83, 248−257.
(21) Gupta, D.; Venugopal, J.; Mitra, S.; Giri Dev, V. R.; Ramakrishna, S. Biomaterials 2009, 30, 2085−2094.
(22) Allo, B. A.; Rizkalla, A. S.; Mequanint, K. Langmuir 2010, 26, 18340−18348.

(23) Stein, G. S.; Lian, J. B.; Stein, J. L.; Van Wijnen, A. J.; Montecino, M. *Physiol. Rev.* **1996**, *76*, 593−629.

(24) Hamamura, K.; Jiang, C.; Yokota, H. *Cell Biol. Int.* **2010**, *34*, 1005−1012.

(25) Idris, S. B.; Bolstad, A. I.; Ibrahim, S. O.; Danmark, S.; Finne-Wistrand, A.; Albertsson, A. C.; Arvidson, K.; Mustafa, K. *Tissue Eng., Part A* **2011**, *17*, 2817−2831.

(26) Alvarez Perez, M. A.; Guarino, V.; Cirillo, V.; Ambrosio, L. *J. Biomed. Mater. Res A* **2012**, *100*, 3008−3019.

(27) Seifu, D. G.; Isimjan, T. T.; Mequanint, K. *Acta Biomater.* **2011**, *7*, 3670−3678.

(28) Kokubo, T.; Kushitani, H.; Sakka, S.; Kitsugi, T.; Yamamuro, T. *J. Biomed. Mater. Res* **1990**, *24*, 721−734.

(29) Allo, B. A.; Rizkalla, A. S.; Mequanint, K. *ACS Appl. Mater. Interfaces* **2012**, *4*, 3148−3156.

(30) Lin, S.; Mequanint, K. *Biomaterials* **2012**, *33*, 7047−7056.

(31) Binulal, N. S.; Deepthy, M.; Selvamurugan, N.; Shalumon, K. T.; Suja, S.; Mony, U.; Jayakumar, R.; Nair, S. V. *Tissue Eng. Part A* **2010**, *16*, 393−404.

(32) Kretlow, J. D.; Mikos, A. G. *Tissue Eng.* **2007**, *13*, 927−938.

(33) Yadav, M. C.; Simao, A. M.; Narisawa, S.; Huesa, C.; McKee, M. D.; Farquharson, C.; Millan, J. L. *J .Bone Miner. Res.* **2011**, *26*, 286−297.

(34) Rosa, A. L.; Beloti, M. M.; van Noort, R. *Dent. Mater.* **2003**, *19*, 768−772.

(35) Boccaccini, A. R.; Erol, M.; Stark, W. J.; Mohn, D.; Hong, Z. K.; Mano, J. F. *Compos. Sci. Technol.* **2010**, *70*, 1764−1776.

(36) Murugan, R.; Ramakrishna, S. *Tissue Eng.* **2006**, *12*, 435−447.

(37) Milleret, V.; Simona, B.; Neuenschwander, P.; Hall, H. *Eur. Cells Mater.* **2011**, *21*, 286−303.

(38) Lee, J. B.; Jeong, S. I.; Bae, M. S.; Yang, D. H.; Heo, D. N.; Kim, C. H.; Alsberg, E.; Kwon, I. K. *Tissue Eng., Part A* **2011**, *17*, 2695−2702.

(39) Kim, H. W.; Kim, H. E.; Knowles, J. C. *Adv. Funct. Mater.* **2006**, *16*, 1529−1535.

(40) Padial-Molina, M.; Galindo-Moreno, P.; Fernández-Barbero, J. E.; O'Valle, F.; Jódar-Reyes, A. B.; Ortega-Vinuesa, J. L.; Ramón-Torregrosa, P. J. *Acta Biomater.* **2011**, *7*, 771−778.

(41) Lucchesi, C.; Ferreira, B. P.; Duek, E. R.; Santos, A., Jr.; Joazeiro, P. *J. Mater. Sci: Mater. Med.* **2008**, *19*, 635−643.

(42) Yun, H. S.; Kim, S. H.; Khang, D. W.; Choi, J. I.; Kim, H. H.; Kang, M. J. *Int. J. Nanomed.* **2011**, *6*, 2521−2531.

(43) Ma, Z.; Kotaki, M.; Yong, T.; He, W.; Ramakrishna, S. *Biomaterials* **2005**, *26*, 2527−2536.

(44) Wang, C.; Wang, M. *J. Mater. Sci. Mater. Med.* **2012**, *23*, 2381−2397.

(45) Tong, H. W.; Wang, M.; Li, Z. Y.; Lu, W. W. *Biomed. Mater.* **2010**, *5*, 054111.

(46) Fujihara, K.; Kotaki, M.; Ramakrishna, S. *Biomaterials* **2005**, *26*, 4139−4147.

(47) Soliman, S.; Pagliari, S.; Rinaldi, A.; Forte, G.; Fiaccavento, R.; Pagliari, F.; Franzese, O.; Minieri, M.; Di Nardo, P.; Licoccia, S.; Traversa, E. *Acta Biomater.* **2010**, *6*, 1227−1237.

(48) Kriegel, C.; Arecchi, A.; Kit, K.; McClements, D. J.; Weiss, J. *Crit. Rev. Food. Sci. Nutr.* **2008**, *48*, 775−797.

(49) Sant, S.; Iyer, D.; Gaharwar, A. K.; Patel, A.; Khademhosseini, A. *Acta Biomater.* **2013**, *9*, 5963−5973.

(50) Samavedi, S.; Olsen Horton, C.; Guelcher, S. A.; Goldstein, A. S.; Whittington, A. R. *Acta Biomater* **2011**, *7*, 4131−4138.

(51) Liu, W.; Yeh, Y.-C.; Lipner, J.; Xie, J.; Sung, H.-W.; Thomopoulos, S.; Xia, Y. *Langmuir* **2011**, *27*, 9088−9093.

(52) Gao, C.; Gao, Q.; Li, Y.; Rahaman, M. N.; Teramoto, A.; Abe, K. *J. Appl. Polym. Sci.* **2013**, *127*, 2588−2599.

(53) Bruning-Fann, C. S.; Kaneene, J. B. *Vet. Hum. Toxicol.* **1993**, *35*, 521−538.

(54) Elias, K. L.; Price, R. L.; Webster, T. J. *Biomaterials* **2002**, *23*, 3279−3287.

(55) Chen, M.; Patra, P. K.; Warner, S. B.; Bhowmick, S. *Tissue Eng.* **2007**, *13*, 579−587.

(56) Isaac, J.; Nohra, J.; Lao, J.; Jallot, E.; Nedelec, J. M.; Berdal, A.; Sautier, J. M. *Eur. Cell Mater.* **2011**, *21*, 130−143.

(57) Siggelkow, H.; Rebenstorff, K.; Kurre, W.; Niedhart, C.; Engel, I.; Schulz, H.; Atkinson, M. J.; Hufner, M. *J. Cell Biochem.* **1999**, *75*, 22−35.

(58) Golub, E. E.; Boesze-Battaglia, K. *Curr. Opin. Orthop.* **2007**, *18*, 444−448.

(59) Aubin, J. E. *J. Cell Biochem. Suppl.* **1998**, *30-31*, 73−82.

(60) Bellows, C. G.; Reimers, S. M.; Heersche, J. N. *Cell Tissue Res.* **1999**, *297*, 249−59.

(61) Thurner, P. J.; Chen, C. G.; Ionova-Martin, S.; Sun, L.; Harman, A.; Porter, A.; Ager, J. W., 3rd; Ritchie, R. O.; Alliston, T. *Bone* **2010**, *46*, 1564−1573.

(62) Razzouk, S.; Brunn, J. C.; Qin, C.; Tye, C. E.; Goldberg, H. A.; Butler, W. T. *Bone* **2002**, *30*, 40−47.

(63) Yang, Y.; Cui, Q.; Sahai, N. *Langmuir* **2010**, *26*, 9848−9859.